The Unfolding Pathway for Apo *Escherichia coli* Aspartate Aminotransferase Is Dependent on the Choice of Denaturant†

Edgar Deu and Jack F. Kirsch*

Department of Molecular and Cell Biology, University of California, Berkeley, Berkeley, California 94720-3206

Received December 21, 2006; Revised Manuscript Received March 7, 2007

ABSTRACT: The guanidine hydrochloride (GdnHCl) mediated denaturation pathway for the apo form of homodimeric *Escherichia coli* aspartate aminotransferase (eAATase) (molecular mass = 43.5 kDa/monomer) includes a partially folded monomeric intermediate, M* [Herold, M., and Kirschner, K. (1990) *Biochemistry 29*, 1907−1913; Birolo, L., Dal Piaz, F., Pucci, P., and Marino, G. (2002) *J. Biol. Chem. 277*, 17428−17437]. The present investigation of the urea-mediated denaturation of eAATase finds no evidence for an M* species but uncovers a partially denatured dimeric form, D*, that is unpopulated in GdnHCl. Thus, the unfolding process is a function of the employed denaturant. D* retains less than 50% of the native secondary structure (circular dichroism), conserves significant quaternary and tertiary interactions, and unfolds cooperatively ($m_{D^*\rightleftarrows U}$ = 3.4 ± 0.3 kcal mol^{-1} M^{-1}). Therefore, the following equilibria obtain in the denaturation of apo-eAATase: D ⇄ 2M ⇄ 2M* ⇄ 2U in GdnHCl and D ⇄ D* ⇄ 2U in urea (D = native dimer, M = folded monomer, and U = unfolded state). The free energy of unfolding of apo-eAATase (D ⇄ 2U) is 36 ± 3 kcal mol^{-1}, while that for the D* ⇄ 2U transition is 24 ± 2 kcal mol^{-1}, both at 1 M standard state and pH 7.5.

Protein folding and structural determinants of stability are two of the most challenging and pursued problems in structural biology. Most of the studies in these areas have been on globular or small multidomain proteins (*1*−*4*) and mainly report on the secondary and tertiary structural organization of monomeric proteins. There have been relatively few investigations of larger oligomeric proteins (*5*), and only some of these provide thermodynamic data (*6*−*12*). Complexities of the folding and unfolding processes increase with protein size. Partially folded conformations (*6*, *9*, *13*−*16*), aggregating species (*6*, *16*, *17*), and/or off-pathway intermediates (*18*, *19*) are often observed for large proteins. Rigorous thermodynamic analyses of multimeric proteins are more complex because both subunit folding and association reactions need to be evaluated.

Numerous quantitative reports of protein complexes formed from native components have appeared. Examples include barnase−barstar (*20*−*23*), antigen−antibody (*24*−*27*), or protein ligand−receptor complexes (*28*−*31*). Obligate oligomeric proteins differ from these systems in that their monomeric constituents do not normally exist as stable folded entities under physiological conditions. Detailed thermodynamic and mutagenesis studies on multimeric proteins are few and are generally limited to very small systems such as coil−coil formation (*32*), the tumor repressor p53 tetramerization domain (*33*), or the 10 kDa P22 Arc repressor homodimer (*34*).

Important diseases such as amyloidoses owe their etiology to protein misfolding and aggregation (*35*−*37*). In some cases, specific mutations are correlated with the stabilities of multimeric proteins. Examples include propionic acidemia and propionyl-CoA carboxylase (*38*) or type II tyrosinemia and tyrosine aminotransferase (*39*).

Escherichia coli aspartate aminotransferase (eAATase)[1] is a platform of sufficient complexity and tractability to probe the stability of a relatively large multimeric protein. It is an 87 kDa obligate homodimer with two pyridoxal 5′-phosphate (PLP) dependent active sites situated at the subunit interface. The monomer is composed of a large (residues 47−329) and a small (residues 5−46 and 330−409) domain (*40*). Most of the intersubunit interactions are between the two large domains, but additional contacts are mediated by the small domain's N-terminal tails that wrap around the opposite large domains. eAATase is the best characterized PLP-dependent enzyme. Its catalytic mechanism has been studied in depth (*41*−*45*), and a variety of crystal structures are available (*40*, *46*−*49*). Site-directed mutagenesis studies have yielded extensive information on substrate specificity (*50*−*54*), cofactor binding (*55*, *56*), and stability (*57*−*60*).

Herold and Kirschner (*61*) thoroughly investigated the guanidine hydrochloride (GdnHCl) mediated denaturation of

† This work was supported NIH Grant GM 35373.

* To whom correspondence should be addressed. Telephone: (510) 642-6368. Fax: (510) 642-6368. E-mail: jfkirsch@berkeley.edu.

[1] Abbreviations: ΔG^0_{unf}, free energy of unfolding at 0 M denaturant; θ_N, normalized ellipticity signal; C_m, denaturant concentration at a transition midpoint; D, native dimeric state; D*, partially folded dimeric intermediate; Den, denaturant; DTT, dithiothreitol; eAATase, *Escherichia coli* aspartate aminotransferase; f_N, normalized fluorescence emission intensity; GdnHCl, guanidine hydrochloride; HEPES, *N*-(2-hydroxyethyl)piperazine-*N*′-2-ethanesulfonic acid; His_6 tag, 6-histidine tag; I, partially folded intermediate; IAEW, intensity-averaged emission wavelength; M, folded monomer; M*, partially folded monomeric intermediate; N, native state; Ni-NTA, nickel nitrilotriacetate; PLP, pyridoxal 5′-phosphate; U, unfolded state; X_{D^*}, mole fraction of D*.

10.1021/bi602621t CCC: $37.00
Published on Web 04/11/2007

the apo form of eAATase and proposed the model of eq 1:

$$D \rightleftarrows 2M \rightleftarrows 2M^* \rightleftarrows 2U \quad (1)$$

where D represents the native apoenzyme; M, a folded monomer; M*, a partially folded monomeric intermediate that has some of the characteristics of a molten globule; and U, the unfolded state. Evidence for M* has also been reported in refs *57* and *58*. M* retains 50% of the secondary structure, is prone to aggregation, and has been considered an off-pathway intermediate (*58*, *62*). Kinetic investigations reveal fast- and slow-folding species as well as multiple-folding intermediates (*13*, *58*, *62*−*64*).

In this work, the stability of eAATase was studied by equilibrium denaturation experiments with both urea and GdnHCl. Although most protein denaturation investigations employing these two denaturants find that the reagents behave similarly (*65*−*68*), we report here that the pathways and the metastable intermediates differ qualitatively for the denaturation of eAATase.

MATERIALS AND METHODS

Cloning, Purification, and Preparation of His_6 Tag Apo-eAATase. The expression (*69*), purification (*70*), and attachment of the 6-histidine tag (His_6 tag) to the C-terminus of eAATase were performed as previously described. Briefly, eAATase was expressed in *E. coli* strain MG204 (a gift from Ian Fotheringham, Nutrasweet Corp,), the cells were disrupted by sonication, and the protein was purified in a single chromatographic step using Ni-NTA Superflow resin (Qiagen, Valencia, CA). Apo-eAATase was prepared in 20 mM potassium phosphate buffer, pH 7.5. Holoenzyme (50 μM) (all enzyme concentrations are given as monomer concentrations) was incubated with 100 mM cysteine sulfinate for 2 h at 25 °C and loaded onto a Ni-NTA Superflow resin, and the cofactor was removed by washing the column with 100 volumes of buffer at 4 °C. Apo-eAATase was eluted with 250 mM imidazole and dialyzed overnight at 4 °C. The decrease of bound cofactor absorbance bands at 330, 360, and 420 nm, as well as the loss of activity, showed that >99% of the enzyme was converted into the apo form.

Folding and Unfolding of Apo-eAATase. (A) Urea. Native apo-eAATase was diluted 10−100-fold into selected concentrations of urea in buffer A (20 mM potassium phosphate, pH 7.5, 1 mM DTT) to final concentrations of 0.5, 2.5, or 10 μM enzyme. Urea concentrations were based on refractive index (*71*, *72*). Unless indicated otherwise, samples were incubated overnight at room temperature, and all measurements were taken at 25 °C. For the refolding experiments, denatured protein, kept for 30 min at 7 M urea in buffer A and 25 °C, was diluted into selected concentrations of urea and incubated as described above.

(*B) GdnHCl.* The incubation conditions were those reported by Herold and Kirschner (*61*): 24 h at 4 °C followed by 1 h at 25 °C in 10 mM HEPES, 5 mM DTT, 1 mM EDTA, and 0−6 M GdnHCl at pH 7.4. The GdnHCl concentrations were determined from the refractive index (*71*).

Spectrophotometric Measurements. (A) Fluorescence. All measurements were performed on a Perkin-Elmer LB50S fluorometer at 25 °C. Samples were excited at 280 nm and emission spectra recorded from 300 to 400 nm. The emission intensities at 365 and 325 nm provide large signal changes for the low and high urea concentration dependent transitions, respectively. For each spectrum, the intensity-averaged emission wavelength (IAEW) was computed with eq 2:

$$\mathrm{IAEW} = \left(\sum_{\lambda=320\mathrm{nm}}^{\lambda=370\mathrm{nm}} F_\lambda \lambda\right) / \left(\sum_{\lambda=320\mathrm{nm}}^{\lambda=370\mathrm{nm}} F_\lambda\right) \quad (2)$$

where F_λ is the fluorescence intensity at the emission wavelength λ.

(*B) Circular Dichroism*. CD measurements were taken on an Aviv 62DS spectrometer with a temperature-controlled cell holder set at 25 °C. The spectra were recorded from 190 to 260 nm, and the ellipticity values were calculated as the average over 1 s nm^{-1}. Path length cuvettes (1 and 0.1 cm) were used for samples containing 0.5 and 10 μM enzyme, respectively. eAATase has a high α-helical content characterized by a band at 222 nm. The loss of secondary structure during unfolding was therefore followed at that wavelength (θ_{222}).

The background signals in fluorescence or CD experiments were measured at seven to nine selected concentrations of denaturant immediately after each data set was collected. The buffer signals, which are linearly dependent on denaturant concentration, were subtracted from the data.

Data Analysis. Table 1 describes the mathematical treatment of unimolecular two-state (*67*) (model I: $N \rightleftarrows U$) and three-state (*73*) (model II: $N \rightleftarrows I \rightleftarrows U$) denaturation models, as well as that of a dimeric protein unfolding through a dimeric intermediate (*6*, *9*, *10*) (model III: $D \rightleftarrows D^* \rightleftarrows 2U$). The last corresponds to the proposed denaturation pathway of apo-eAATase in urea. For all models, the free energies associated with each equilibrium constant were assumed to be linearly dependent on denaturant concentration (linear extrapolation method) (*72*, *74*). Models I and II were used to calculate C_m values (Table 1, eq 11). CD data were treated according to model II and fluorescence data according to model I, because each transition was monitored at a different emission wavelength. The intrinsic signals for all species were assumed to be linearly dependent on denaturant concentration. A null slope (α_i in Table 1, eq 12) was assigned either when the associated error was greater than the parameter value or when there were insufficient data points to determine the parameter accurately. All models were fitted to eq 12 by nonlinear regression analysis with the KaleidaGraph program for models I and II and with the NLIN program of the SAS statistical package (SAS Institute, Cary, NC) for model III.

RESULTS

Reversible Urea-Mediated Denaturation of Apo-eAATase. (A) Intrinsic Fluorescence Measurements. Figure 1 shows the dependence of tryptophan fluorescence on denaturant concentration. The emission intensity increases slightly from 2 to 3 M urea, and the IAEW shifts from 343 to 345 nm. The intensity decreases back to the initial level between 4 and 6 M urea, and IAEW shifts further to 348 nm (insets in Figure 1). These observations identify an intermediate in the urea-mediated denaturation of apo-eAATase.

Because of the small changes in emission intensity, no single wavelength provides a sufficiently good signal-to-noise

Table 1: Equations Describing the Thermodynamic Treatment of Different Protein Denaturation Models[a]

Model I $N \rightleftarrows U$	**Model II** $N \rightleftarrows I \rightleftarrows U$	**Model III** $D \rightleftarrows D^* \rightleftarrows 2U$	Eq
$K_{N\rightleftarrows U} = \frac{[U]}{[N]}$	$K_{N\rightleftarrows I} = \frac{[I]}{[N]}$; $K_{I\rightleftarrows U} = \frac{[U]}{[I]}$	$K_{D\rightleftarrows D^*} = \frac{[D^*]}{[D]}$; $K_{D^*\rightleftarrows 2U} = \frac{[U]^2}{[D^*]}$	3
$P_T = [N] + [U]$	$P_T = [N] + [I] + [U]$	$P_T = 2[D] + 2[D^*] + [U]$	4
$X_N = \frac{[N]}{P_T}$; $X_U = \frac{[U]}{P_T}$	$X_N = \frac{[N]}{P_T}$; $X_I = \frac{[I]}{P_T}$; $X_U = \frac{[U]}{P_T}$	$X_D = \frac{2[D]}{P_T}$; $X_{D^*} = \frac{2[D^*]}{P_T}$; $X_U = \frac{[U]}{P_T}$	5
$\sum_i X_i = 1$			6
$K_{N\rightleftarrows U} = \frac{X_U}{X_N}$	$K_{N\rightleftarrows I} = \frac{X_I}{X_N}$; $K_{I\rightleftarrows U} = \frac{X_U}{X_I}$	$K_{D\rightleftarrows D^*} = \frac{X_{D^*}}{X_D}$; $K_{D^*\rightleftarrows 2U} = \frac{2P_T X_U^2}{X_{D^*}}$	7
$X_N = \frac{1}{1+K_{N\rightleftarrows U}}$	$X_N = \frac{1}{1+K_{N\rightleftarrows I}+K_{N\rightleftarrows I}K_{I\rightleftarrows U}}$	$X_D = \frac{4P_T(1+K_{D\rightleftarrows D^*}) + K_{D\rightleftarrows D^*}K_{D^*\rightleftarrows 2U} - \sqrt{(K_{D\rightleftarrows D^*}K_{D^*\rightleftarrows 2U})^2 + 8P_T K_{D\rightleftarrows D^*}K_{D^*\rightleftarrows 2U}(1+K_{D\rightleftarrows D^*})}}{4P_T(1+K_{D\rightleftarrows D^*})^2}$	8
$X_U = \frac{K_{N\rightleftarrows U}}{1+K_{N\rightleftarrows U}}$	$X_I = \frac{K_{N\rightleftarrows I}}{1+K_{N\rightleftarrows I}+K_{N\rightleftarrows I}K_{I\rightleftarrows U}}$	$X_{D^*} = (K_{D\rightleftarrows D^*}) \frac{4P_T(1+K_{D\rightleftarrows D^*}) + K_{D\rightleftarrows D^*}K_{D^*\rightleftarrows 2U} - \sqrt{(K_{D\rightleftarrows D^*}K_{D^*\rightleftarrows 2U})^2 + 8P_T K_{D\rightleftarrows D^*}K_{D^*\rightleftarrows 2U}(1+K_{D\rightleftarrows D^*})}}{4\cdot P_T\cdot(1+K_{D\rightleftarrows D^*})^2}$	9
	$X_U = \frac{K_{N\rightleftarrows I}K_{I\rightleftarrows U}}{1+K_{N\rightleftarrows I}+K_{N\rightleftarrows I}K_{I\rightleftarrows U}}$	$X_U = \frac{-K_{D\rightleftarrows D^*}K_{D^*\rightleftarrows 2U} + \sqrt{(K_{D\rightleftarrows D^*}K_{D^*\rightleftarrows 2U})^2 + 8\cdot P_T K_{D\rightleftarrows D^*}K_{D^*\rightleftarrows 2U}(1+K_{D\rightleftarrows D^*})}}{4P_T(1+K_{D\rightleftarrows D^*})}$	10
$K_{j\rightleftarrows k} = \exp\left(m_{j\rightleftarrows k}\,([Den] - C_{m,j\rightleftarrows k})/RT\right)$		$K_{j\rightleftarrows k} = \exp\left(-(\Delta G^0_{j\rightleftarrows k} - m_{j\rightleftarrows k}\,[Den])/RT\right)$	11
$S = \sum_i (S_i^0 + \alpha_i[Den])\ X_i$			12

[a] Equations 3: equilibria. Equations 4: mass conservation (P_T is the total monomer concentration). Equations 5: mole fraction definitions. Equations 7: equilibrium constants defined in mole fractions. Equations 8−10: mole fractions expressed as a function of the equilibrium constants and P_T (obtained from eqs 6 and 7). Equations 11: expressions of the equilibrium constants according to the linear extrapolation method; [Den] is the concentration of denaturant, $\Delta G^0_{j\rightleftarrows k}$ is the free energy associated with the equilibrium constant $K_{j\rightleftarrows k}$ at [Den] = 0 M, $m_{j\rightleftarrows k}$ is the cooperativity parameter for the $j \rightleftarrows k$ transition, and $C_{m,j\rightleftarrows k}$ is the [Den] at the transition midpoint. Equation 12: general equation that describes the dependence of an observable, S, on [Den]. S_i^0 is the intrinsic S value at [Den] = 0 M for state i, and α_i represents the dependence of S_i on [Den].

ratio to monitor both transitions. The wavelengths 365 and 325 nm, which provide a significantly large change in intensity, were chosen to observe the formation and disappearance of the intermediate, respectively (Figure 1). Fully unfolded apo-eAATase was diluted into selected concentrations of denaturant and incubated overnight at 25 °C, and the extent of renaturation was monitored by fluorescence as described above. Figure 1 and Table 2 show that the unfolding and refolding curves at 10 μM enzyme and their associated C_m values are identical within experimental error. Therefore, the extent of unfolding in these experiments does reflect equilibrium conditions.

While the first step ($C_{m,D\rightleftarrows D^*} \sim 2.5$ M urea) is independent within experimental error of enzyme concentration, the second transition clearly shifts to higher denaturant concentration as the protein concentration is increased (Figure 1). The error in $C_{m,D\rightleftarrows D^*}$ at 0.5 μM enzyme is ±0.2 M urea; this midpoint value does not differ significantly from those obtained at higher protein concentrations (Table 2). Additionally, IAEW (Figure 1, inset B) and CD (See below) measurements clearly show that the transition at lower urea concentrations is enzyme concentration independent. The first step thus corresponds to a unimolecular process, and the second measures the dimer to monomers equilibrium. The simplest model that accommodates these results is one in which the native dimer undergoes an initial urea-dependent transformation to a dimeric intermediate (D*) prior to its dissociation into two unfolded monomers at higher urea concentrations (eq 13):

$$D \rightleftarrows D^* \rightleftarrows 2U \qquad (13)$$

D* is the only species that is significantly populated between 3 and 4 M urea. Its tryptophans are partially solvent exposed as only one-third of the total red shift is observed during the D ⇄ D* transition (Figure 1, inset B) (*75*).

(*B) Circular Dichroism.* The CD data, monitored by θ_{222} (Figure 2), also show an enzyme concentration independent step followed by a concentration dependent transition, in agreement with the model of eq 13. Table 2 shows that the C_m values obtained by fluorescence and CD are equal within experimental error for each enzyme concentration. It is of interest that the protein remains a dimer even after 60% of the secondary structure is lost as indicated by θ_{222}.

Global Fitting of Apo-eAATase Denaturation Parameters in Urea Solutions. The dependence of the intrinsic signal for each species on denaturant concentration (S_i^0 and α_i parameters defined in Table 1) was evaluated by fitting the fluorescence and CD data to eq 12 for models I and II, respectively (Figures 1 and 2). The resultant S_i^0 and α_i values were fixed in eq 12 to globally fit all of the data to model III. Table 2 reports the obtained stability parameters for apo-

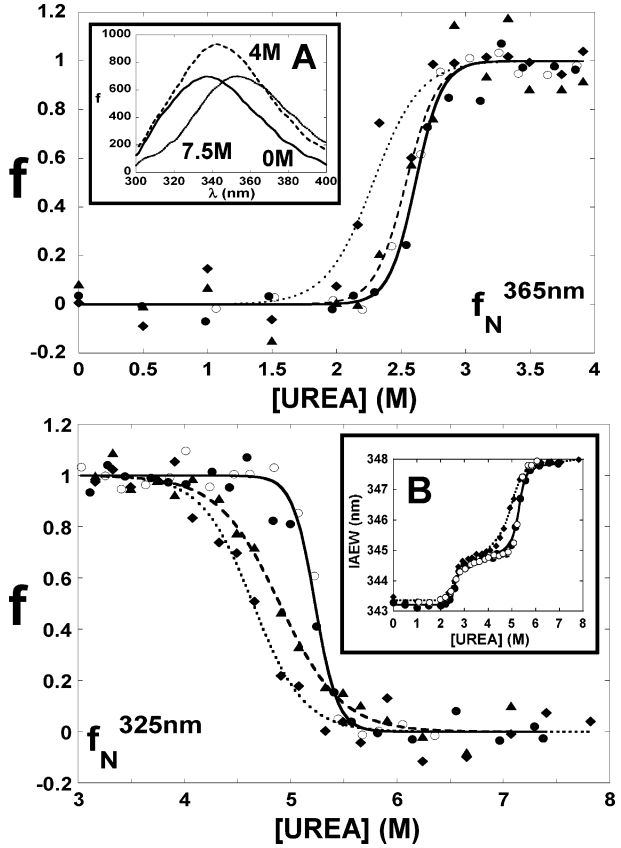

FIGURE 1: Apo-eAATase fluorescence as a function of urea concentration. eAATase samples were incubated overnight at 25 °C in buffer A containing 0−8 M urea. Emission spectra were recorded from 300 to 400 nm (λ_{ex} = 280 nm). The normalized emissions at 365 and 325 nm (upper and lower panels, respectively) are shown for 0.5 (◆), 2.5 (▲), and 10 μM [(●) unfolding; (○) refolding] apo-eAATase. The refolding experiment was performed by diluting completely unfolded enzyme (at 7 M urea) into buffer A containing the indicated denaturant concentrations. The dotted, dashed, and solid lines show the fit to eq 12, model I (Table 1), for the data obtained at 0.5, 2.5, and 10 μM enzyme, respectively. Inset A shows the emission spectra of 10 μM enzyme at the specified urea concentrations, and inset B shows the dependence of IAEW on urea concentration at 0.5 [unfolding (◆)] and 10 μM [unfolding (●) and refolding (○)] apo-eAATase. IAEW fits were computed with eq 12, model II (Table 1).

eAATase. The accuracy of the fit is illustrated in Figure 3: at all enzyme and urea concentrations the mole fraction of D* (X_{D^*}) was computed from the experimental data with eqs 14 and 15 (points in Figure 3) and compared with the simulated X_{D^*} calculated with eq 9 of model III (Table 1):

$$X_{D^*} = \frac{S - (S^0_D + \alpha_D[\text{urea}])}{(S^0_{D^*} + \alpha_{D^*}[\text{urea}]) - (S^0_D + \alpha_D[\text{urea}])} \quad [\text{urea}] < 3.2\ \text{M} \quad (14)$$

$$X_{D^*} = \frac{S - (S^0_U + \alpha_U[\text{urea}])}{(S^0_{D^*} + \alpha_{D^*}[\text{urea}]) - (S^0_U + \alpha_U[\text{urea}])} \quad [\text{urea}] \geq 3.2\ \text{M} \quad (15)$$

The m values reported in Table 2 clearly show that both transitions are cooperative. The total free energy of unfolding (ΔG^0_{unf}) of apo-eAATase is 36 ± 3 kcal mol^{-1} at 1 M standard state. This value is comparable with those obtained

Table 2: C_m, m, and ΔG^0 Values Describing the Denaturation of the Apo-eAATase Dimer[a]

probe	[enzyme] (μM)	$C_{m,D\rightleftarrows D^*}$ (M)	$C_{m,D^*\rightleftarrows 2U}$ (M)
fluorescence	10	2.61 (0.03)	5.19 (0.04)
fluorescence	10[b]	2.60 (0.03)	5.26 (0.04)
fluorescence	2.5	2.5 (0.1)	4.9 (0.1)
fluorescence	0.5	2.3 (0.2)	4.6 (0.1)
CD	10	2.50 (0.03)	5.24 (0.06)
CD	0.5	2.53 (0.05)	4.6 (0.2)

Global Fit[c]

standard state	$\Delta G^0_{D\rightleftarrows D^*}$ (kcal mol^{-1})	$m_{D\rightleftarrows D^*}$ (kcal mol^{-1} M^{-1})	$\Delta G^0_{D^*\rightleftarrows 2U}$ (kcal mol^{-1})	$m_{D^*\rightleftarrows 2U}$ (kcal mol^{-1} M^{-1})
1 M	12 (2)	4.8 (0.8)	24.4 (0.8)	3.4 (0.2)
1 μM	12 (2)	4.8 (0.8)	16.2 (0.6)	3.4 (0.2)

[a] The fluorescence and CD parameters were obtained from eq 12 (Table 1), models I and II, respectively. [b] Renaturation experiment. [c] Obtained from globally fitting all of the data to eq 12 of model III (Table 1).

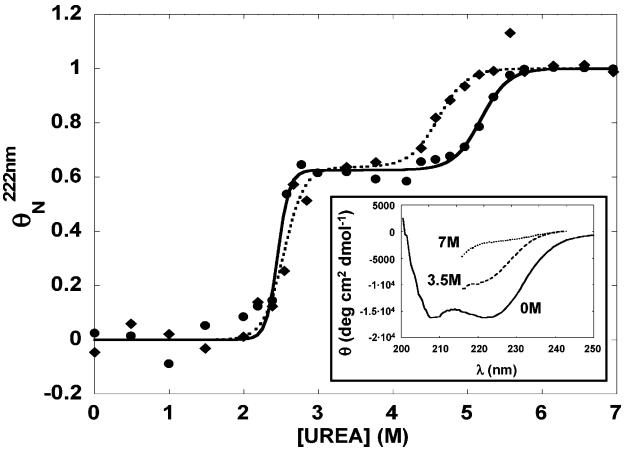

FIGURE 2: Molar ellipticity of apo-eAATase in urea. The normalized θ_{222} values of 0.5 (◆) and 10 μM (●) apo-eAATase samples following overnight incubation at 25 °C in buffer A at the indicated concentrations of urea are shown. The dotted and solid lines show the fit to eq 12, model II (Table 1), for the data obtained at 0.5 and 10 μM enzyme, respectively. The inset shows illustrative CD spectra of 10 μM enzyme incubated at different urea concentrations.

for other dimeric proteins for which dimeric intermediates are reported. Examples include bacterial luciferase (*16*), tyrosyl-tRNA synthetase (*10*), and organophosphorus hydrolase (*6*), whose ΔG^0_{unf} are 28, 27, and 44 kcal mol^{-1}, respectively.

Denaturation of Apo-eAATase in GdnHCl. All results obtained with urea as the denaturant are consistent with the existence of a dimeric intermediate in the denaturation of apo-eAATase. However, Herold and Kirschner (*61*) showed that the unfolding pathway of the same protein in GdnHCl follows a reversible four-state model, where the native dimer dissociates to folded monomers, followed by conversion to a monomeric intermediate (M*) that unfolds to the fully denatured state (eq 1).

The main difference in the experimental conditions is that Herold and Kirschner (*61*) employed a different denaturant, but they also incubated the enzyme for 24 h at 4 °C followed by 1 h at 25 °C (10 mM HEPES, pH 7.4, 5 mM DTT, 1 mM EDTA, and 0−6 M GdnHCl). The urea denaturation experiments reported here included overnight incubation at

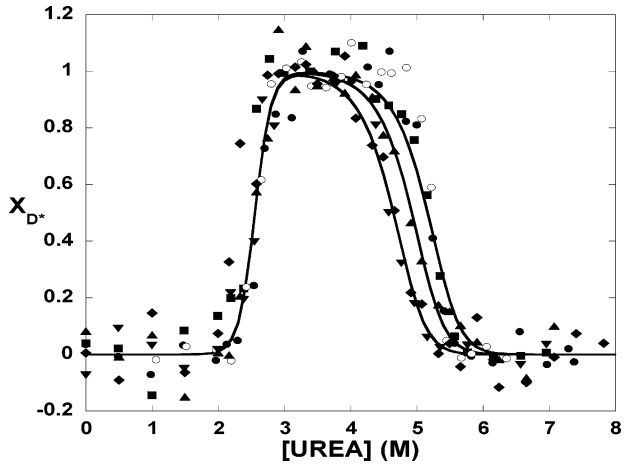

FIGURE 3: Mole fraction of the dimeric intermediate, X_{D^*}, as a function of urea and enzyme concentration. X_{D^*} calculated from the CD (▼, ■) and fluorescence data (eqs 14 and 15) at 0.5 (◆, ▼), 2.5 (▲), and 10 μM (●, ■; ○, refolding) are compared to the calculated X_{D^*} from the ΔG^0 and m values reported in Table 2 with eq 9 of model III (Table 1).

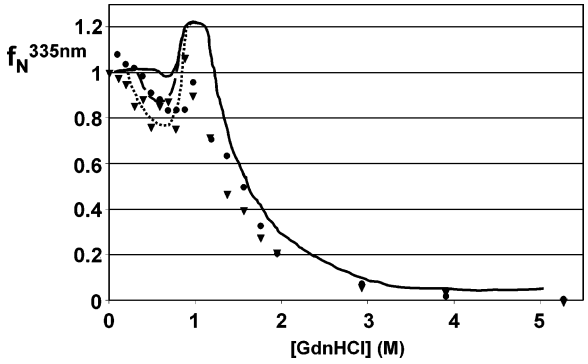

FIGURE 4: GdnHCl denaturation of 0.1 (▼) and 4 μM (●) His_6-tagged apo-eAATase in GdnHCl monitored by fluorescence emission at 335 nm (λ_{ex} = 280 nm). Samples containing 0−6 M GdnHCl were incubated 24 h at 4 °C followed by 1 h at 25 °C in 10 mM HEPES, 5 mM DTT, and 1 mM EDTA at pH 7.4. The lines show the denaturation curves reported by Herold and Kirschner (*61*) under the same incubation conditions for 0.09 (dotted line), 0.39 (dashed line), and 3.9 μM (solid line) enzyme.

25 °C (20 mM potassium phosphate, pH 7.5, 1 mM DTT, and 0−8 M urea). Additionally, the enzyme used in the present study contains a C-terminal His_6 tag. A combination of one or more of the experimental variations is thus responsible for the qualitatively distinct intermediates described in eqs 1 and 13.

To attempt to discover the reason(s) for the differing results, 0.1 and 4 μM His_6-tagged apo-eAATase was incubated in GdnHCl under the conditions reported in ref *61*. The extent of unfolding was followed by fluorescence at 335 nm with excitation at 280 nm. Figure 4 compares the denaturation curves obtained with the His_6-eAATase (Figure 4, data points) vs those obtained in ref *61* (Figure 4, lines).

The data sets are very similar and appear to show three transitions. The decrease of the emission intensity from 0 to 0.5 M GdnHCl is enzyme concentration dependent and corresponds to the D $\rightleftarrows$ 2M dissociation process. The second transition, characterized by an increase of the emission intensity from 0.5 to 1 M GdnHCl, corresponds to the formation of M*. Finally, the gradual decrease of fluorescence between 1 and 4 M GdnHCl reports the unfolding of

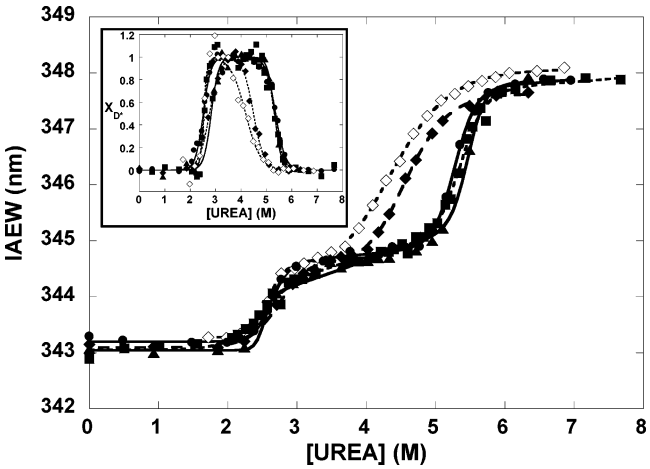

FIGURE 5: Dependence of the urea-mediated denaturation curve on incubation temperature. 10 μM apo-eAATase was incubated at low (4 °C, 24 h) and/or high (25 °C, 12 h) temperatures in buffer A. The IAEW and molar fraction of dimeric intermediate, X_{D^*} (inset), are shown for the following incubation schedules: 24 h at 4 °C [(◆) denaturation; (◇) renaturation], 12 h at 25 °C (●), 24 h at 4 °C followed by 12 h at 25 °C (▲), and 12 h at 25 °C followed by 24 h at 4 °C (■). X_{D^*} was calculated from eqs 14 and 15 as explained in Materials and Methods. The individual data sets were fitted to eq 12 of model II (Table 1).

M*. Therefore, the His_6 tag is not responsible for the differing denaturation pathways.

Effect of Temperature on the Apo-eAATase Unfolding Pathway. The temperature effect on the urea-mediated denaturation of 10 μM apo-eAATase was evaluated after incubation at 4 °C (24 h) and 25 °C (12 h) in 0−8 M urea in buffer A. The effects of these single incubations or their combinations, low temperature followed by high temperature and vice versa, are shown in the fluorescence-monitored denaturation curves of Figure 5. The low-temperature samples were incubated for 5 min at 25 °C prior to fluorescence measurements.

The renaturation curves at 4 °C (Figure 5) and 25 °C (Figure 1) are almost identical to the corresponding denaturation curves, thus proving that equilibrium was established at both temperatures. While the first denaturation step is independent of the incubation temperature, the midpoint of the second transition decreases from 5.2 M at 25 °C to 4.5 M urea at 4 °C (Figure 5). Although the incubation temperature has an effect on the dissociation step, it does not alter the unfolding mechanism of apo-eAATase (eq 13).

To test the interconvertibility between the 4 and 25 °C equilibria, the effects of combining the two denaturation conditions were investigated. Incubation at 25 °C of samples that had reached the 4 °C equilibrium yielded a denaturation curve in agreement with the 25 °C equilibrium (Figure 5). However, the curve obtained after incubation at 4 °C of samples that had reached the 25 °C equilibrium point is superimposable to the one obtained after a single 25 °C incubation. Thus samples in the D* state at 25 °C are kinetically trapped when transferred at 4 °C and cannot reach the unfolded state, which is a more stable conformation at that temperature (see Discussion).

These results show that the urea denaturation pathway is the same at 4 and 25 °C (eq 13). Thus, the two distinct partially folded intermediates observed for apo-eAATase are a function of the chemical denaturant only and are not

significantly perturbed by either the incubation temperature or the His_6 tag. The effect of temperature on GdnHCl denaturation could not be studied due to the formation of an aggregating intermediate at 25 °C (*61*).

DISCUSSION

Nature of the Dimeric Intermediate. The urea-mediated equilibrium denaturation of apo-eAATase reveals the presence of a dimeric intermediate that retains only 40% of the native secondary structure. Additionally, the *m* values (Table 2) indicate that ~50% of the buried surface area is exposed upon D* formation. Dimeric intermediates in unfolding have only been reported for a handful of proteins: bacterial luciferase (*9*, *16*, *18*), histone-like HU protein (*76*), procaspase-3 (*14*), glutathione transferase (*15*), 3-isopropylmalate dehydrogenase (*77*), and human growth hormone (*78*). Others appear to be directly linked to amyloid formation (*79*−*81*). An intermediate similar to the one described here has been reported for organophosphorus hydrolase (*6*) and SecA (*17*).

The denaturation curves of apo-eAATase in urea show two well-defined cooperative transitions, indicative of two independently unfolding structural regions with unequal stabilities. As the dissociation step takes place at higher urea concentrations, D* must retain the key intersubunit contacts. The eAATase dimeric interface is composed of interactions across the two large domains as well as contacts between the N-terminal tails and the large domains [PDB entry 1ASN (*40*)]. A truncated eAATase construct lacking the small domain forms a compact inactive monomer that still binds PLP (*19*). Thus, the N-terminal tails are probably essential for dimer formation and might be part of the structural region that unfolds at higher urea concentrations.

The ΔG^0 values (Table 2) calculated for a 1 M standard state indicate that the D* $\rightleftarrows$ 2U transition accounts for two-thirds (24.4 kcal mol^{-1}) of ΔG^0_{unf} (36 kcal mol^{-1}). At a more realistic 1 μM standard state, $\Delta G^0_{D^* \rightleftarrows 2U}$ is 16.2 kcal mol^{-1} and the total ΔG^0_{unf} is 28 kcal mol^{-1}.

The Denaturant Determines the Unfolding Pathways. The traditionally accepted view of the equivalence of urea and GdnHCl as denaturants is based predominantly on experiments performed on monomeric globular proteins (*65*−*67*), whose hydrophobic cores account for most of their stability. However, other denaturant-dependent unfolding pathways have been documented. In most cases, the unfolding mechanisms change from two-state in urea to three-state in GdnHCl (*82*−*87*). Stabilization of a partially folded state (*83*), or relaxation of the native conformation through specific binding of guanidinium ions to negatively charged pockets, and/or shielding of repulsive electrostatic interactions (*84*−*86*) are some of the proposed explanations for the appearance of an additional intermediate. Additionally, Monera et al. (*88*) showed that, in contrast to urea, measurements obtained from GdnHCl-mediated denaturation do not reflect the contribution of electrostatic interactions to the stability of coiled coils. The unequal ability of urea and guanidinium ion to disrupt electrostatic interactions has also been noted (*89*−*91*).

Interactions with low concentrations of GdnHCl preferentially destabilize the apo-eAATase dimer, and/or stabilize M*, leading to the accumulation of the latter, while those with urea unveil a partially structured dimer. The present results differ from those described above in that each denaturant stabilizes a structurally differentiated intermediate. The CD data reported by Herold and Kirschner (*61*) show that M* retains 50% of the secondary structure observed in the native form; however, D* has even less secondary structure (40%). Further, as judged by the changes in λ_{max} (Figure 1, inset A), the tryptophans are more exposed to the solvent in D* than in M* (one-third vs one-fifth of the total red shift, respectively). Finally, M* has some molten globule characteristics and unfolds less cooperatively than does D*, which retains significant tertiary and quaternary interactions. These structural differences make it very unlikely that these two intermediates could coexist in the same unfolding pathway.

Protein interfaces contain more polar interactions than do the interiors of monomeric proteins. Therefore, the mechanisms by which the two denaturants perturb quaternary structure are likely to differ. Indeed, several studies on multimeric proteins have reported significantly different stability results that depend on the nature of the denaturant (*6*, *12*, *82*, *85*, *92*). Eighty-five percent of the eAATase interactions (defined by a 4 Å cutoff) across the large domain side chains are hydrogen bonds or salt bridges, while 43% of the N-terminal arm's intersubunit contacts are hydrophobic. Thus, the predominance of polar interactions might explain why an ionic denaturant like GdnHCl is more effective at disrupting the apo-eAATase interface than is urea.

Bypassing the Dimeric Intermediate during Unfolding. The effect of temperature on the denaturation of apo-eAATase (Figure 5) shows that at intermediate urea concentrations (ca. 4.5−5 M) U and D* are the most stable species at 4 and 25 °C, respectively. D*, which is populated at 4−5 M urea and 25 °C, becomes trapped in this state as dropping the temperature to 4 °C does not shift the transition to that observed when the entire denaturation process is carried out at 4 °C (Figure 5).

These observations are illustrated by the reaction coordinate profiles shown in Figure 6 for 10 μM apo-eAATase in 5 M urea. Under the above-described incubation conditions, a solution of native dimer (D) transferred to 5 M urea at 25 or 4 °C populates the most thermodynamically stable species, i.e., D* and U, respectively. The unfolded monomer obtained at 5 M urea and 4 °C reverts to D* when transferred to 25 °C. However, reducing the temperature at 5 M urea from 25 to 4 °C does not produce the D* → U reaction as would be expected. The barriers for reverting to D or U are too high, and D* is trapped as a kinetically stable but thermodynamically unstable species (Figure 6, right panel). The native dimer placed in 5 M urea at 4 °C bypasses D* and proceeds directly to 2U (Figure 6).

In summary, these experiments demonstrate that the type of denaturant may qualitatively change the nature of the partially folded populated intermediates in unfolding pathways. In the case of eAATase, GdnHCl disrupts quaternary interactions more strongly than does urea. Given the complexities of the folding and assembly processes of oligomeric proteins, the use of an alternative denaturant may populate intermediates that are not otherwise observed or thermodynamically favor one or more of the multiple partially folded species present in a rugged energetic landscape of a protein folding funnel (*3*). For example, the stabilization of D* by

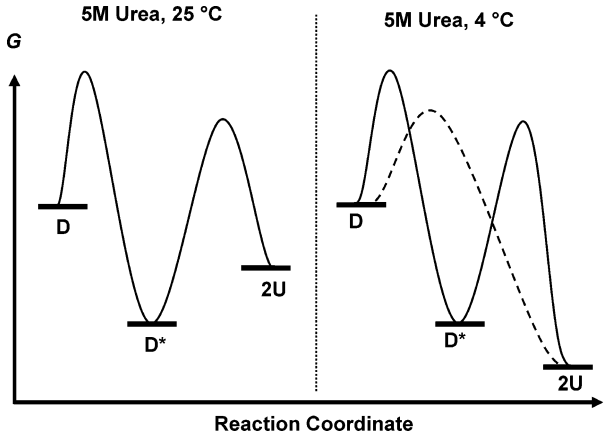

FIGURE 6: D*, formed at 25 °C in 5 M urea, is kinetically trapped at 4 °C. Reaction coordinate profiles of 10 μM apo-eAATase in 5 M urea (buffer A) at 25 and 4 °C are shown in the left and right panels, respectively. The absolute heights of the transition states are arbitrary, but the relative heights in each panel are qualitatively significant. The solid lines represent the simplest unfolding trajectories that include D* as an on-pathway intermediate. Although the D* $\rightleftarrows$ 2U equilibrium becomes favored at 4 °C, that and the D* $\rightarrow$ D kinetic barriers cannot be traversed in 24 h. The dashed line shows an alternative pathway from D $\rightarrow$ U that bypasses D* and thus reaches the most stable species at 4 °C.

urea might allow the monitoring of the so far elusive dimerization step during eAATase folding.

ACKNOWLEDGMENT

We thank Dr. Keith A. Koch for the cloning of His_6-tagged eAATase and Dr. Katie Tripp for thoughtful comments and helpful suggestions on the manuscript.

REFERENCES

1. Dagget, V., and Fersht, A. (2003) The present view of the mechanism of protein folding, *Nat. Rev. 4*, 497−502.
2. Englander, S. W., Mayne, L., and Rumbley, J. N. (2002) Submolecular cooperativity produces multi-state protein unfolding and refolding, *Biophys. Chem. 101*−*102*, 57−65.
3. Onuchic, J. N., and Wolynes, P. G. (2004) Theory of protein folding, *Curr. Opin. Struct. Biol. 14*, 70−75.
4. Bai, Y. (2003) Hidden intermediates and Levinthal paradox in the folding of small proteins, *Biochem. Biophys. Res. Commun. 305*, 785−788.
5. Neet, K. E., and Timm, D. E. (1994) Conformational stability of dimeric proteins: quantitative studies by equilibrium denaturation, *Protein Sci. 3*, 2167−2174.
6. Grimsley, J. K., Scholtz, J. M., Pace, C. N., and Wild, J. R. (1997) Organophosphorus hydrolase is a remarkably stable enzyme that unfolds through a homodimeric intermediate, *Biochemistry 36*, 14366−14374.
7. Gloss, L. M., and Placek, B. J. (2002) The effect of salts on the stability of the H2A-H2B histone dimer, *Biochemistry 41*, 14951−14959.
8. Hobart, S. A., Ilin, S., Moriarty, D. F., Osuna, R., and Colon, W. (2002) Equilibrium denaturation studies of the *Escherichia coli* factor for inversion stimulation: implications for *in vivo* function, *Protein Sci. 11*, 1671−1680.
9. Clark, A. C., Sinclair, J. F., and Baldwin, T. O. (1993) Folding of bacterial luciferase involves a non-native heterodimeric intermediate in equilibrium with the native enzyme and the unfolded subunits, *J. Biol. Chem. 268*, 10773−10779.
10. Park, Y. C., and Bedouelle, H. (1998) Dimeric tyrosyl-tRNA synthetase from *Bacillus stearothermophilus* unfolds through a monomeric intermediate. A quantitative analysis under equilibrium conditions, *J. Biol. Chem. 273*, 18052−18059.
11. Wojciak, P., Mazurkiewicz, A., Bakalova, A., and Kuciel, R. (2003) Equilibrium unfolding of dimeric human prostatic acid phosphatase involves an inactive monomeric intermediate, *Int. J. Biol. Macromol. 32*, 43−54.
12. Hornby, J. A., Luo, J. K., Stevens, J. M., Wallace, L. A., Kaplan, W., Armstrong, R. N., and Dirr, H. W. (2000) Equilibrium folding of dimeric class mu glutathione transferases involves a stable monomeric intermediate, *Biochemistry 39*, 12336−12344.
13. Oses-Prieto, J. A., Bengoechea-Alonso, M. T., Artigues, A., Iriarte, A., and Martinez-Carrion, M. (2003) The nature of the rate-limiting steps in the refolding of the cofactor-dependent protein aspartate aminotransferase, *J. Biol. Chem. 278*, 49988−49999.
14. Bose, K., and Clark, A. C. (2001) Dimeric procaspase-3 unfolds via a four-state equilibrium process, *Biochemistry 40*, 14236−14242.
15. Stevens, J. M., Hornby, J. A., Armstrong, R. N., and Dirr, H. W. (1998) Class sigma glutathione transferase unfolds via a dimeric and a monomeric intermediate: impact of subunit interface on conformational stability in the superfamily, *Biochemistry 37*, 15534−15541.
16. Inlow, J. K., and Baldwin, T. O. (2002) Mutational analysis of the subunit interface of *Vibrio harveyi* bacterial luciferase, *Biochemistry 41*, 3906−3915.
17. Doyle, S. M., Braswell, E. H., and Teschke, C. M. (2000) SecA folds via a dimeric intermediate, *Biochemistry 39*, 11667−11676.
18. Clark, A. C., Raso, S. W., Sinclair, J. F., Ziegler, M. M., Chaffotte, A. F., and Baldwin, T. O. (1997) Kinetic mechanism of luciferase subunit folding and assembly, *Biochemistry 36*, 1891−1899.
19. Herold, M., Leistler, B., Hage, A., Luger, K., and Kirschner, K. (1991) Autonomous folding and coenzyme binding of the excised pyridoxal 5′-phosphate binding domain of aspartate aminotransferase from *Escherichia coli*, *Biochemistry 30*, 3612−3620.
20. Frisch, C., Fersht, A. R., and Schreiber, G. (2001) Experimental assignment of the structure of the transition state for the association of barnase and barstar, *J. Mol. Biol. 308*, 69−77.
21. Dalby, P. A., Clarke, J., Johnson, C. M., and Fersht, A. R. (1998) Folding intermediates of wild-type and mutants of barnase. II. Correlation of changes in equilibrium amide exchange kinetics with the population of the folding intermediate, *J. Mol. Biol. 276*, 647−656.
22. Dalby, P. A., Oliveberg, M., and Fersht, A. R. (1998) Folding intermediates of wild-type and mutants of barnase. I. Use of phi-value analysis and m-values to probe the cooperative nature of the folding pre-equilibrium, *J. Mol. Biol. 276*, 625−646.
23. Dalby, P. A., Oliveberg, M., and Fersht, A. R. (1998) Movement of the intermediate and rate determining transition state of barnase on the energy landscape with changing temperature, *Biochemistry 37*, 4674−4679.
24. Pons, J., Rajpal, A., and Kirsch, J. F. (1999) Energetic analysis of an antigen/antibody interface: alanine scanning mutagenesis and double mutant cycles on the HyHEL-10/lysozyme interaction, *Protein Sci. 8*, 958−968.
25. Sundberg, E. J., and Mariuzza, R. A. (2002) Molecular recognition in antibody-antigen complexes, *Adv. Protein Chem. 61*, 119−160.
26. Pons, J., Stratton, J. R., and Kirsch, J. F. (2002) How do two unrelated antibodies, HyHEL-10 and F9.13.7, recognize the same epitope of hen egg-white lysozyme?, *Protein Sci. 11*, 2308−2315.
27. Fuh, G., Wu, P., Liang, W. C., Ultsch, M., Lee, C. V., Moffat, B., and Wiesmann, C. (2006) Structure-function studies of two synthetic anti-vascular endothelial growth factor Fabs and comparison with the Avastin Fab, *J. Biol. Chem. 281*, 6625−6631.
28. Nickel, J., Dreyer, M. K., Kirsch, T., and Sebald, W. (2001) The crystal structure of the BMP-2:BMPR-IA complex and the generation of BMP-2 antagonists, *J. Bone Joint Surg. Am. 83-A* (Suppl. 1), S7−S14.
29. Duchesnes, C. E., Murphy, P. M., Williams, T. J., and Pease, J. E. (2006) Alanine scanning mutagenesis of the chemokine receptor CCR3 reveals distinct extracellular residues involved in recognition of the eotaxin family of chemokines, *Mol. Immunol. 43*, 1221−1231.
30. McFarland, B. J., Kortemme, T., Yu, S. F., Baker, D., and Strong, R. K. (2003) Symmetry recognizing asymmetry: analysis of the interactions between the C-type lectin-like immunoreceptor NKG2D and MHC class I-like ligands, *Structure 11*, 411−422.
31. Zhang, J. L., Foster, D., and Sebald, W. (2003) Human IL-21 and IL-4 bind to partially overlapping epitopes of common gamma-chain, *Biochem. Biophys. Res. Commun. 300*, 291−296.
32. Yu, Y. B. (2002) Coiled-coils: stability, specificity, and drug delivery potential, *Adv. Drug Deliv. Rev. 54*, 1113−1129.

33. Mateu, M. G., Sanchez, Del, Pino, M. M., and Fersht, A. R. (1999) Mechanism of folding and assembly of a small tetrameric protein domain from tumor suppressor p53, *Nat. Struct. Biol. 6*, 191−198.
34. Sauer, R. T., Milla, M. E., Waldburger, C. D., Brown, B. M., and Schildbach, J. F. (1996) Sequence determinants of folding and stability for the P22 Arc repressor dimer, *FASEB J. 10*, 42−48.
35. Scheibel, T., and Buchner, J. (2006) Protein aggregation as a cause for disease, *Handb. Exp. Pharmacol.* 199−219.
36. Soto, C., Estrada, L., and Castilla, J. (2006) Amyloids, prions and the inherent infectious nature of misfolded protein aggregates, *Trends Biochem. Sci. 31*, 150−155.
37. May, B. C., Govaerts, C., and Cohen, F. E. (2006) Developing therapeutics for the diseases of protein misfolding, *Neurology 66*, S118−S122.
38. Desviat, L. R., Perez, B., Perez-Cerda, C., Rodriguez-Pombo, P., Clavero, S., and Ugarte, M. (2004) Propionic acidemia: mutation update and functional and structural effects of the variant alleles, *Mol. Genet. Metab. 83*, 28−37.
39. Charfeddine, C., Monastiri, K., Mokni, M., Laadjimi, A., Kaabachi, N., Perin, O., Nilges, M., Kassar, S., Keirallah, M., Guediche, M. N., Kamoun, M. R., Tebib, N., Ben, Dridi, M. F., Boubaker, S., Ben, Osman, A., and Abdelhak, S. (2006) Clinical and mutational investigations of tyrosinemia type II in Northern Tunisia: identification and structural characterization of two novel TAT mutations, *Mol. Genet. Metab. 88*, 184−191.
40. Jager, J., Moser, M., Sauder, U., and Jansonius, J. N. (1994) Crystal structures of *Escherichia coli* aspartate aminotransferase in two conformations. Comparison of an unliganded open and two liganded closed forms, *J. Mol. Biol. 239*, 285−305.
41. Velick, S. F., and Vavra, J. (1962) A kinetic and equilibrium analysis of the glutamic oxaloacetate transaminase mechanism, *J. Biol. Chem. 237*, 2109−2122.
42. Kirsch, J. F., Eichele, G., Ford, G. C., Vincent, M. G., Jansonius, J. N., Gehring, H., and Christen, P. (1984) Mechanism of action of aspartate aminotransferase proposed on the basis of its spatial structure, *J. Mol. Biol. 174*, 497−525.
43. Eliot, A. C., and Kirsch, J. F. (2004) Pyridoxal phosphate enzymes: mechanistic, structural, and evolutionary considerations, *Annu. Rev. Biochem. 73*, 383−415.
44. Sandmeier, E., and Christen, P. (1980) Mitochondrial aspartate aminotransferase 27/32-410. Partially active enzyme derivative produced by limited proteolytic cleavage of native enzyme, *J. Biol. Chem. 255*, 10284−10289.
45. Goldberg, J. M., and Kirsch, J. F. (1996) The reaction catalyzed by *Escherichia coli* aspartate aminotransferase has multiple partially rate-determining steps, while that catalyzed by the Y225F mutant is dominated by ketimine hydrolysis, *Biochemistry 35*, 5280−5291.
46. Jager, J., Pauptit, R. A., Sauder, U., and Jansonius, J. N. (1994) Three-dimensional structure of a mutant *E. coli* aspartate aminotransferase with increased enzymatic activity, *Protein Eng. 7*, 605−612.
47. Okamoto, A., Higuchi, T., Hirotsu, K., Kuramitsu, S., and Kagamiyama, H. (1994) X-ray crystallographic study of pyridoxal 5′-phosphate-type aspartate aminotransferases from *Escherichia coli* in open and closed form, *J. Biochem. (Tokyo) 116*, 95−107.
48. Kamitori, S., Okamoto, A., Hirotsu, K., Higuchi, T., Kuramitsu, S., Kagamiyama, H., Matsuura, Y., and Katsube, Y. (1990) Three-dimensional structures of aspartate aminotransferase from *Escherichia coli* and its mutant enzyme at 2.5 Å resolution, *J. Biochem. (Tokyo) 108*, 175−184.
49. Miyahara, I., Hirotsu, K., Hayashi, H., and Kagamiyama, H. (1994) X-ray crystallographic study of pyridoxamine 5′-phosphate-type aspartate aminotransferases from *Escherichia coli* in three forms, *J. Biochem. (Tokyo) 116*, 1001−1012.
50. Danishefsky, A. T., Onufer, J. J., Petsko, G. A., and Ringe, D. (1991) Activity and structure of the active-site mutants R386Y and R386F of *Escherichia coli* aspartate aminotransferase, *Biochemistry 30*, 1980−1985.
51. Inoue, Y., Kuramitsu, S., Inoue, K., Kagamiyama, H., Hiromi, K., Tanase, S., and Morino, Y. (1989) Substitution of a lysyl residue for arginine 386 of *Escherichia coli* aspartate aminotransferase, *J. Biol. Chem. 264*, 9673−9681.
52. Onuffer, J. J., and Kirsch, J. F. (1995) Redesign of the substrate specificity of *Escherichia coli* aspartate aminotransferase to that of *Escherichia coli* tyrosine aminotransferase by homology modeling and site-directed mutagenesis, *Protein Sci. 4*, 1750−1757.
53. Rothman, S. C., Voorhies, M., and Kirsch, J. F. (2004) Directed evolution relieves product inhibition and confers in vivo function to a rationally designed tyrosine aminotransferase, *Protein Sci. 13*, 763−772.
54. Rothman, S. C., and Kirsch, J. F. (2003) How does an enzyme evolved *in vitro* compare to naturally occurring homologs possessing the targeted function? Tyrosine aminotransferase from aspartate aminotransferase, *J. Mol. Biol. 327*, 593−608.
55. Toney, M. D., and Kirsch, J. F. (1991) Kinetics and equilibria for the reactions of coenzymes with wild type and the Y70F mutant of *Escherichia coli* aspartate aminotransferase, *Biochemistry 30*, 7461−7466.
56. Toney, M. D., and Kirsch, J. F. (1991) Tyrosine 70 fine-tunes the catalytic efficiency of aspartate aminotransferase, *Biochemistry 30*, 7456−7461.
57. Birolo, L., Malashkevich, V. N., Capitani, G., De Luca, F., Moretta, A., Jansonius, J. N., and Marino, G. (1999) Functional and structural analysis of cis-proline mutants of *Escherichia coli* aspartate aminotransferase, *Biochemistry 38*, 905−913.
58. Birolo, L., Dal Piaz, F., Pucci, P., and Marino, G. (2002) Structural characterization of the M* partly folded intermediate of wild type and P138A aspartate aminotransferase from *Escherichia coli*, *J. Biol. Chem. 277*, 17428−17437.
59. Gloss, L. M., Planas, A., and Kirsch, J. F. (1992) Contribution to catalysis and stability of the five cysteines in *Escherichia coli* aspartate aminotransferase. Preparation and properties of a cysteine-free enzyme, *Biochemistry 31*, 32−39.
60. Gloss, L. M., Spencer, D. E., and Kirsch, J. F. (1996) Cysteine-191 in aspartate aminotransferases appears to be conserved due to the lack of a neutral mutation pathway to the functional equivalent, alanine-191, *Proteins 24*, 195−208.
61. Herold, M., and Kirschner, K. (1990) Reversible dissociation and unfolding of aspartate aminotransferase from *Escherichia coli*: characterization of a monomeric intermediate, *Biochemistry 29*, 1907−1913.
62. Leistler, B., Herold, M., and Kirschner, K. (1992) Collapsed intermediates in the reconstitution of dimeric aspartate aminotransferase from *Escherichia coli*, *Eur. J. Biochem. 205*, 603−611.
63. Reyes, A. M., Iriarte, A., and Martinez-Carrion, M. (1993) Refolding of the precursor and mature forms of mitochondrial aspartate aminotransferase after guanidine hydrochloride denaturation, *J. Biol. Chem. 268*, 22281−22291.
64. Artigues, A., Iriarte, A., and Martinez-Carrion, M. (1997) Refolding intermediates of acid-unfolded mitochondrial aspartate aminotransferase bind to hsp70, *J. Biol. Chem. 272*, 16852−16861.
65. Greene, R. F., Jr., and Pace, C. N. (1974) Urea and guanidine hydrochloride denaturation of ribonuclease, lysozyme, alpha-chymotrypsin, and beta-lactoglobulin, *J. Biol. Chem. 249*, 5388−5393.
66. Ahmad, F., and Bigelow, C. C. (1982) Estimation of the free energy of stabilization of ribonuclease A, lysozyme, alpha-lactalbumin, and myoglobin, *J. Biol. Chem. 257*, 12935−12938.
67. Santoro, M. M., and Bolen, D. W. (1988) Unfolding free energy changes determined by the linear extrapolation method. 1. Unfolding of phenylmethanesulfonyl alpha-chymotrypsin using different denaturants, *Biochemistry 27*, 8063−8068.
68. Bolen, D. W., and Santoro, M. M. (1988) Unfolding free energy changes determined by the linear extrapolation method. 2. Incorporation of delta G degrees N-U values in a thermodynamic cycle, *Biochemistry 27*, 8069−8074.
69. Onuffer, J. J., and Kirsch, J. F. (1994) Characterization of the apparent negative co-operativity induced in *Escherichia coli* aspartate aminotransferase by the replacement of Asp222 with alanine. Evidence for an extremely slow conformational change, *Protein Eng. 7*, 413−424.
70. Deu, E., Koch, K. A., and Kirsch, J. F. (2002) The role of the conserved Lys68*:Glu265 intersubunit salt bridge in aspartate aminotransferase kinetics: multiple forced covariant amino acid substitutions in natural variants, *Protein Sci. 11*, 1062−1073.
71. Nozaki, Y. (1972) The preparation of guanidine hydrochloride, *Methods Enzymol. 26* (Part C), 43−50.
72. Pace, C. N. (1986) Determination and analysis of urea and guanidine hydrochloride denaturation curves, *Methods Enzymol. 131*, 266−280.
73. Barrick, D., and Baldwin, R. L. (1993) Three-state analysis of sperm whale apomyoglobin folding, *Biochemistry 32*, 3790−3796.
74. Pace, C. N., and Shaw, K. L. (2000) Linear extrapolation method of analyzing solvent denaturation curves, *Proteins* (Suppl. 4), 1−7.

75. Lakowicz, J. R. (1983) *Principles of Fluorescence Spectroscopy*, Plenum Press, New York.
76. Ramstein, J., Hervouet, N., Coste, F., Zelwer, C., Oberto, J., and Castaing, B. (2003) Evidence of a thermal unfolding dimeric intermediate for the *Escherichia coli* histone-like HU proteins: thermodynamics and structure, *J. Mol. Biol. 331*, 101−121.
77. Motono, C., Yamagishi, A., and Oshima, T. (1999) Urea-induced unfolding and conformational stability of 3-isopropylmalate dehydrogenase from the thermophile thermus thermophilus and its mesophilic counterpart from *Escherichia coli*, *Biochemistry 38*, 1332−1337.
78. Kasimova, M. R., Milstein, S. J., and Freire, E. (1998) The conformational equilibrium of human growth hormone, *J. Mol. Biol. 277*, 409−418.
79. Zhu, L., Zhang, X. J., Wang, L. Y., Zhou, J. M., and Perrett, S. (2003) Relationship between stability of folding intermediates and amyloid formation for the yeast prion Ure2p: a quantitative analysis of the effects of pH and buffer system, *J. Mol. Biol. 328*, 235−254.
80. Rodziewicz-Motowidlo, S., Wahlbom, M., Wang, X., Lagiewka, J., Janowski, R., Jaskolski, M., Grubb, A., and Grzonka, Z. (2006) Checking the conformational stability of cystatin C and its L68Q variant by molecular dynamics studies: why is the L68Q variant amyloidogenic?, *J. Struct. Biol. 154*, 68−78.
81. Eakin, C. M., Attenello, F. J., Morgan, C. J., and Miranker, A. D. (2004) Oligomeric assembly of native-like precursors precedes amyloid formation by beta-2 microglobulin, *Biochemistry 43*, 7808−7815.
82. Zhou, J. M., Fan, Y. X., Kihara, H., Kimura, K., and Amemiya, Y. (1997) Unfolding of dimeric creatine kinase in urea and guanidine hydrochloride as measured using small angle X-ray scattering with synchrotron radiation, *FEBS Lett. 415*, 183−185.
83. Morjana, N. A., McKeone, B. J., and Gilbert, H. F. (1993) Guanidine hydrochloride stabilization of a partially unfolded intermediate during the reversible denaturation of protein disulfide isomerase, *Proc. Natl. Acad. Sci. U.S.A. 90*, 2107−2111.
84. Mayr, L. M., and Schmid, F. X. (1993) Stabilization of a protein by guanidinium chloride, *Biochemistry 32*, 7994−7998.
85. Akhtar, M. S., Ahmad, A., and Bhakuni, V. (2002) Guanidinium chloride- and urea-induced unfolding of the dimeric enzyme glucose oxidase, *Biochemistry 41*, 3819−3827.
86. Pace, C. N., Laurents, D. V., and Thomson, J. A. (1990) pH dependence of the urea and guanidine hydrochloride denaturation of ribonuclease A and ribonuclease T1, *Biochemistry 29*, 2564−2572.
87. Del Vecchio, P., Graziano, G., Granata, V., Farias, T., Barone, G., Mandrich, L., Rossi, M., and Manco, G. (2004) Denaturant-induced unfolding of the acetyl-esterase from *Escherichia coli*, *Biochemistry 43*, 14637−14643.
88. Monera, O. D., Kay, C. M., and Hodges, R. S. (1994) Protein denaturation with guanidine hydrochloride or urea provides a different estimate of stability depending on the contributions of electrostatic interactions, *Protein Sci. 3*, 1984−1991.
89. Monera, O. D., Kay, C. M., and Hodges, R. S. (1994) Electrostatic interactions control the parallel and antiparallel orientation of alpha-helical chains in two-stranded alpha-helical coiled-coils, *Biochemistry 33*, 3862−3871.
90. Monera, O. D., Zhou, N. E., Kay, C. M., and Hodges, R. S. (1993) Comparison of antiparallel and parallel two-stranded alpha-helical coiled-coils. Design, synthesis, and characterization, *J. Biol. Chem. 268*, 19218−19227.
91. Pace, C. N. (1990) Conformational stability of globular proteins, *Trends Biochem. Sci. 15*, 14−17.
92. Bhatt, A. N., Prakash, K., Subramanya, H. S., and Bhakuni, V. (2002) Different unfolding pathways for mesophilic and thermophilic homologues of serine hydroxymethyltransferase, *Biochemistry 41*, 12115−12123.

BI602621T